Article

Gypsum-Enhanced Red Mud Composites: A Study on Strength, Durability, and Leaching Characteristics

Shiying Yan, Yu Cheng, Wentong Wang *, Lu Jin and Ziyi Ding

College of Transportation, Shandong University of Science and Technology, Qingdao 266510, China; yanshiying@sdust.edu.cn (S.Y.); skd996718@sdust.edu.cn (Y.C.); skd991767@sdust.edu.cn (L.J.); dzy@sdust.edu.cn (Z.D.)
* Correspondence: wwt@sdust.edu.cn

Abstract: The strong alkalinity of red mud and the heavy metals it contains pose a serious threat to the environment. This study investigated the possibility of applying red mud as a solid waste material in road construction to mitigate the problem of red mud accumulation. Red mud was modified using titanium gypsum and phosphogypsum as curing agents. The effects of varying gypsum types and mixing ratios on the mechanical properties and heavy metal leaching of the resulting red mud-based materials were assessed using percussion tests, unconfined compressive strength measurements, scanning electron microscopy (SEM), and continuous heavy metal leaching tests. The results showed that the optimal moisture content for titanium gypsum–cement-stabilized red mud (RTC) exceeds that of phosphogypsum–cement-stabilized red mud (RPC), with RTC exhibiting a lower maximum dry density compared to RPC. When the gypsum admixture was within 10%, the strength of the RPC was higher than that of the RTC at the same and curing time. The reticulation in RPC-10 was denser. The cumulative heavy metal releases from both RTC and RPC were within the permissible limits for Class III groundwater discharge standards. Based on the comprehensive test results, RPC is identified as the superior modified red mud material, with an optimal mix ratio of red mud/phosphogypsum/cement of 87:5:8.

Keywords: red mud; gypsum; mechanical properties; microstructure; heavy metal leaching

1. Introduction

The rapid development of transportation construction in China has led to an increasing demand for roadbed filling materials in recent years. Since traditional roadbed materials consume a large amount of non-renewable soil resources, research on the use of solid wastes as roadbed fill materials has attracted widespread attention. China is a large alumina-producing country, and for every 1 ton of alumina produced, approximately 0.6 to 2.0 tons of red mud is generated [1]. The annual discharge of red mud is close to 150 million tons, and the cumulative discharge has exceeded 1.3 billion tons, making red mud the largest pollutant discharged from alumina plants. At present, the global red mud reserves are estimated to have exceeded 3 billion tons, the average utilization rate of red mud in the world is 15%, and the utilization rate of red mud in China is only 4% [2]. Red mud is highly productive, strongly alkaline, has a high risk of pollutant migration, and contains radioactive and toxic substances, and its massive accumulation not only occupies land resources but also leads to serious social and ecological environmental problems [3–5]. Therefore, there is an urgent need to find a suitable treatment for red mud, which can be solidified and used as roadbed filler, to realize the sustainable development of the alumina industry and reduce the impact of red mud on the socio-economic and ecological environment.

At present, domestic and foreign scientists' research on the resource utilization of red mud has three main directions: firstly, the mining and extraction of valuable metals;

secondly, the production of building materials such as building bricks; and thirdly, the use of red mud as an adsorbent for wastewater treatment, especially for radioactive metal ions [6–9]. There are also some studies on the use of red mud as an adsorbent for heavy metal ions to treat soils contaminated with heavy metals. Xie et al. [10] investigated the stabilizing and curing effects of a red mud–fly ash composite curing agent on Cu^{2+} containing loess, and the results showed that this composite curing agent was able to rapidly adsorb Cu^{2+}, and at the same time, it enabled the Cu^{2+} to form $Cu(OH)_2$ precipitation in an alkaline environment, which effectively inhibited the migration of Cu^{2+}. Santona et al. [11] and Liang et al. [12] also stated in their studies that red mud can effectively reduce the solubility of heavy metals in contaminated soils. In addition, Sutar et al. [13] stated in their study that the application of red mud in construction materials, pollution control, and metal recycling all require quite high conditions and need to consider the risk of introducing new pollutants; therefore, more in-depth studies on red mud are needed, as well as a comprehensive assessment of the chemical and biological impacts it produces. Sarath et al. [14] replaced red mud with fly ash added gypsum to the mix and set up a mix ratio for strength and heavy metal leaching tests, which illustrated that fly ash and gypsum can significantly increase the strength of red mud and reduce the leaching of most heavy metals. Li et al. [15] stated that the degradation of bonding behavior due to the chloride-induced corrosion of steel strands is critical for the serviceability of prestressed concrete structures. Zhang et al. [16] studied the leaching of heavy metals from fly ash-based cementitious materials containing arsenic. Tests have shown that the solidification/stabilization technology for municipal solid waste incineration can effectively reduce the leaching of heavy metals from most fly ash-based cementitious materials containing arsenic.

The physical properties and composition of red mud are similar to those of soil, and the use of cured red mud as a roadbed filler can provide an effective way for the comprehensive utilization of red mud. Li et al. [17] investigated the synergistic effects of industrial solid wastes in ternary cementless composites based on red mud, ultra-fine fly ash, and ground granulated blast-furnace slag. The results showed that the addition of RM to the cementless composite led to reduced fluidity and compressive strength, as well as prolonged setting times. Deelwal [18] showed that red mud is denser and stronger compared to soil, and the cohesion of red mud is higher than that of conventional clay materials, so it can be used as a geotechnical material such as backfill, road base material, and embankment material, and it can be further stabilized by using lime, gypsum, and fly ash to improve its strength. Shi et al. [19] and Yu [20] verified the feasibility of cement–lime–phosphogypsum-cured red mud applied to road subgrade through indoor tests of road properties such as unconfined compressive strength and splitting resistance. Li [21] selected cement, lime, and phosphogypsum as the curing agents, using the indoor test and field test on the curing of red mud used as a roadbed filler. The results showed that the curing agent could improve the performance of red mud very well, but the improvement effects were greatly influenced by the admixture. The comprehensive use of cement, lime, and phosphogypsum curing of red mud is better than the curing of cement only, which can also cause excessive thermal fatigue [22]. Pu et al. [23] showed in their study that gypsum can improve the engineering utilization of soils and can be more effective when it is synergistic with cement. Li et al. [24] demonstrated experimentally that the Ca^{2+} in gypsum can react with silicate to form calcium silicate hydrate (C-S-H) or silica–aluminate groups, which improve the mechanical properties of terracotta-based grouting materials. Suo [25] and his workers used red mud and desulfurization gypsum to prepare cementitious materials, and their experiments proved that the addition of red mud and desulfurization gypsum can improve the performance of composite soils, and that the optimum ratio of desulfurization gypsum and red mud is 2:2. Zhang et al. [26] and Zhang et al. [27] investigated the mechanical properties of composite fillers using red mud and desulfurization gypsum as raw materials, and the results showed that red mud and desulfurization gypsum can promote the hydration reaction and improve the strength of the modified materials. In the above study, it can be seen that there is a great risk in using pure red mud as a roadbed

filler, and because of the technology and cost, the utilization rate of red mud is very low. Therefore, there is a significant problem in terms of large-scale consumption.

In view of these, this paper selected titanium gypsum and phosphogypsum as curing agents, designed material mixing ratios, and investigated the effects of different gypsums and mixing ratios on the mechanical properties of red mud-based materials using indoor tests such as compaction tests, unconfined compressive strength, and SEM to explore the feasibility of using red mud-based materials for road filling materials. Meanwhile, since the geotechnical environmental evaluation of red mud is difficult and there is no mature research and relevant standard specification, this paper derives the data related to the leaching of heavy metal ions from red mud-based materials through the continuous heavy metal flume leaching test and evaluates the environmental safety of the groundwater of red mud used as a filling material based on the "Standard for groundwater quality" (GB/T 14848-2017) [28]. Finally, the test results were analyzed to propose the optimal material mix ratio that meets both the mechanical requirements of road subgrade materials and the requirements of groundwater standards. This provides a basis for applying red mud to road construction and solving the problem of red mud stockpiling.

2. Materials and Methods

2.1. Materials

2.1.1. Red Mud

The red mud used in the tests was selected from the Shandong Binzhou Beihai red mud dump. The original red mud was air-dried red mud, and its appearance was red lumps. Depending on the quality of the red mud required for the tests, the lumpy red mud was first air-dried, pulverized in a pulverizer, then dried at 105 °C to a constant weight and ground through a 0.075 mm square hole sieve. Its basic physical properties were investigated. The basic physical properties are shown in Table 1.

Table 1. Basic physical properties of red mud specimens.

Plastic Limit/%	Liquid Limit/%	The Natural Moisture Content/%	Optimum Moisture Content ω/%	Maximum Dry Density/g·cm^{-3}	pH
27.4	17.21	35.9	24.1	1.82	10.49

The chemical composition and content in the red mud specimens from the Beihai were detected using X-ray fluorescence spectrometry, as shown in Table 2. The mineral composition of red mud mainly includes SiO_2, Fe_2O_3, $Al_2Si_2O_5(OH)_4$, $Mg_2CO_3(OH)_2(H_2O)_3$, and $AlO(OH)$.

Table 2. Main chemical composition and content of red mud.

Composition	SiO$_2$	Fe$_2$O$_3$	Al$_2$O$_3$	CaO	MgO	TiO$_2$	Na$_2$O	K$_2$O	Other
Content/wt%	28.09	25.54	19.81	1.71	0.29	2.15	10.17	0.31	11.43

2.1.2. Titanium Gypsum

The titanium gypsum required for the tests came from Jinan Yuxing Chemical Co., Ltd. (Jinan, China) and was sticky, reddish, and shaped like clay. The chemical composition and content in the titanium gypsum specimens was detected using an X-ray fluorescence spectrometer, as shown in Table 3. The mineral composition of the titanium gypsum mainly consisted of $CaSO_4$-$2H_2O$, Fe_2O_3, and SiO_2.

Table 3. Main chemical composition and content of titanium gypsum.

Composition	CaO	SO$_3$	Fe$_2$O$_3$	TiO$_2$	SiO$_2$	Na$_2$O	Al$_2$O$_3$	Other
Content/t%	27.43	34.42	9.28	5.49	4.34	1.13	1.37	0.786

2.1.3. Phosphogypsum

The phosphogypsum powder used for the tests was from Linyi Schkofen Chemical Co. Ltd., (Linyi, China) and its appearance was a light gray powder. The chemical composition and content in the phosphogypsum specimens were detected using X-ray fluorescence spectrometry, as shown in Table 4. The main mineral compositions of the phosphogypsum were CaSO$_4$-2H$_2$O, SiO$_2$, etc.

Table 4. Main chemical compositions and contents of phosphogypsum.

Composition	SO$_3$	P$_2$O$_5$	Al$_2$O$_3$	SiO$_2$	CaO	Other
Content/%	52.29	1.23	1.02	6.76	37.53	1.17

2.1.4. Cement

The ordinary silicate benchmark cement used in the tests was from Qufu Zhonglian Cement Co., Ltd. (Qufu, China) and had a dark gray appearance. The basic physical properties of the benchmark cement are shown in Table 5, and the chemical composition analysis results are shown in Table 6. The main mineral compositions of the cement were C$_3$S, C$_2$S, C$_4$AF, and CA.

Table 5. Physical properties of benchmark cement.

Fineness 0.08/% [1]	Specific Surface Area m^2/kg	Density g/cm^3	Solidification Time (min)		Flexural Strength (MPa)		Compressive Strength (MPa)	
			Initial Set	Final Set	3 days	7 days	3 days	7 days
0.4	345	3.12	95	156	6.3	7.8	28.0	39.5

[1] Percentage of sieve residue from a 0.08 mm square-hole sieve.

Table 6. Chemical composition and content of benchmark cement.

Composition	SO$_2$	Al$_2$O$_3$	Fe$_2$O$_3$	CaO	MgO	SO$_3$	Na$_2$O	f-CaO [1]	Cl$^-$	Other
Content/%	20.12	5.12	3.62	63.56	2.07	2.38	0.53	0.75	0.015	2.06

[1] Calcium oxide in a free state.

2.2. Specimen Preparation

A fixed cement admixture of 8%, along with titanium gypsum and phosphogypsum admixtures of 0%, 3%, 5%, 7%, and 10%, were used to prepare standard-sized specimens with a diameter of 39.1 mm and height of 80 mm at room temperature and pressure. The mass of the specimen was calculated according to the optimum moisture content and maximum dry density obtained from the compaction test results. The specimens were prepared according to 96% compaction. After the specimens were made, they were sealed in a Ziplock bag and placed in the curing room. The temperature of the curing room was controlled at 20 ± 2 °C, the relative humidity was controlled at 95%, and the curing ages were 7 d, 14 d, and 28 d. The specimen preparation process is shown in Figure 1. The titanium gypsum–cement-stabilized red mud matrix composites (RTC) and phosphogypsum–cement-stabilized red mud matrix composites (RPC) mix ratios are shown in Table 7.
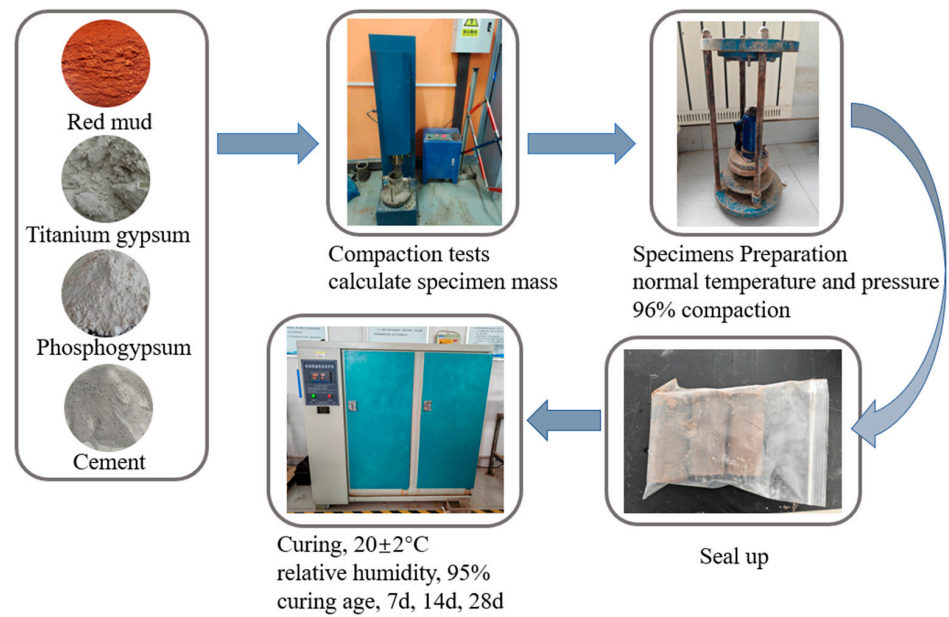
Figure 1. The specimen preparation process.

Table 7. RTC and RPC mix ratios.

Number	Admixture/%			Number	Admixture/%		
	Red Mud	Titanium Gypsum	Cement		Red Mud	Phospho Gypsum	Cement
RTC-0	92	0	8	RPC-0	92	0	8
RTC-3	89	3	8	RPC-3	89	3	8
RTC-5	87	5	8	RPC-5	87	5	8
RTC-7	85	7	8	RPC-7	85	7	8
RTC-10	82	10	8	RPC-10	82	10	8

2.3. Experimental Methods

2.3.1. Compaction Test

The compaction test was carried out using a standard (electric) compaction apparatus, and a compaction cylinder with an inner diameter of 10 cm and a height of 12.7 cm was selected according to the heavy compaction test method of soil in the "Test Methods of Soils for Highway Engineering" (JTG 3430-2020) [29]. The test was carried out three times, and the average value was taken as the test result.

2.3.2. Unconfined Compressive Strength

The unconfined compressive strength test was carried out based on "Test Methods of Soils for Highway Engineering" (JTG 3430-2020) [29]. The microcomputer-controlled electronic universal testing machine (WDW-S100 type) was used to control the loading speed of 1 mm/min. The specimens were prepared according to the compaction degree of 96%, and the unconfined compressive strength test was carried out when the curing age reached 7 d, 14 d, and 28 d, respectively. Three parallel specimens were set up for each group, and the average value was taken as the result of unconfined compressive strength.

2.3.3. Scanning Electron Microscopy (SEM)

The equipment used in this experiment was the ApreoSHiVac field emission scanning electron microscope. Before the experiment, the test block was knocked to the appropriate size, and a block sample with a relatively smooth surface was taken and dried to a constant weight in an oven at 105 °C. After removing the sample, it was placed in a drying tower

until the sample was cooled to room temperature. The carbon conductive adhesive was first affixed to the sample stage, and then the sample was fixed to the conductive adhesive to ensure that the sample was firmly affixed to the sample stage. After fixing the sample, the sample was sprayed with gold, then the sample was observed and analyzed by selecting the appropriate magnification.

2.3.4. Continuous Flume Leaching Test

According to the block leaching test specification NEN 7375-2004 [30], a block sample of 4 cm × 4 cm × 16 cm was made using pure water in the laboratory as the leaching solution with a liquid–solid ratio of 10 L/kg. Eight consecutive cycles of leaching tests were conducted on the cement-stabilized red mud materials (RTC-0, RPC-0, and RC) and gypsum–cement-stabilized red mud matrix composites with different admixtures. At the end of each leaching stage, we measured the concentration of heavy metals in the leach solution. To minimize the experimental error, three groups of parallel tests were set up, and the test results were averaged to further analyze the leaching pattern of the heavy metals [31]. Figure 2 shows the continuous water tank leaching test setup in this paper, and Table 8 shows the leaching solution replacement time of the continuous water tank leaching test.
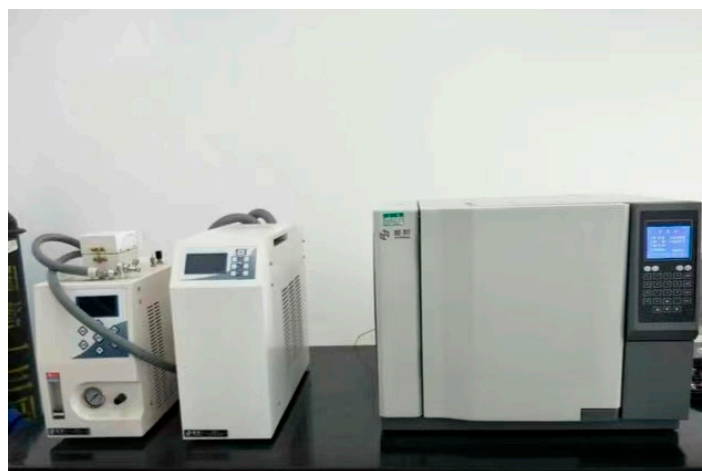

Figure 2. Continuous flume leaching test setup.

Table 8. Leach solution replacement time.

Leach Stage	Leach Solution Replacement Time	
	Cumulative Time/d	Interval Time/h
1	0.25	6
2	1	18
3	2.25	30
4	4	42
5	9	120
6	16	168
7	36	480
8	64	672

The following is the method of data processing used for the continuous flume leaching test NEN 7375-2004 [32]:

(1) The amount of a component leached E_i obtained for each stage i is shown in Equation (1):

$$E_i = \frac{V_i \times C_i}{m_d} \tag{1}$$

In the equation:

E_i: the amount of a component leached in the leaching stage i, mg/kg;
C_i: concentration of a component in the leach solution at leaching stage i, mg/L;
m_d: mass of sample dry matter in the column, kg.

(2) The leaching concentration E_i^* of a component obtained for each stage i is shown in Equation (2):

$$E_i^* = \frac{V_i \times C_i}{f \times A} \tag{2}$$

In the equation:

E_i^*: leaching concentration of a component at leaching stage i, mg/m^2;
V_i: volume of leach solution at leaching stage i, L;
C_i: concentration of a component in the leach solution at leaching stage i, μg/L;
f: a conversion factor, 1000 μg/mg;
A: surface area of the sample.

(3) The cumulative release of a component U_n is calculated as shown in Equation (3):

$$U_n = \sum_{i=1}^{8} E_i \tag{3}$$

In the equation:

U_n: cumulative leaching of a component in stages 1–8, mg/kg;
E_i: the amount of a component leached at the leaching stage i, mg/kg.

3. Results and Analysis

3.1. Comparative Analysis of Optimum Moisture Content and Maximum Dry Density

The RTC and RPC with different mixing ratios were subjected to compaction tests to obtain their optimum moisture contents and maximum dry densities. as shown in Table 9. Figure 3 shows the compaction characteristic curves of the cement-stabilized red mud-based materials with different gypsum types and different mixing ratios. Based on the figure, the optimal moisture content was less affected by the gypsum type and material ratio, and the optimal moisture content of the different gypsum-modified red mud composites was concentrated at 22~27%. In Figure 3a, the peak of the compaction curve gradually shifted to the lower right with the increase in the titanium gypsum admixture, the maximum dry density of RTC decreased with the increase in the titanium gypsum admixture by 0.11 g/cm^3, and the optimum moisture content increased with the increase in the titanium gypsum admixture by 0.87%. In Figure 3b, the peak of the compaction curve shifted irregularly with the increase in the phosphogypsum admixture. In this case, the optimum moisture content of RTC is slightly greater than that of RPC, and the maximum dry density of RTC is slightly less than that of RPC, which is caused by the fact that the water absorption of titanium gypsum is slightly greater than that of phosphogypsum.

Table 9. Compaction test results of composites with different mix ratios.

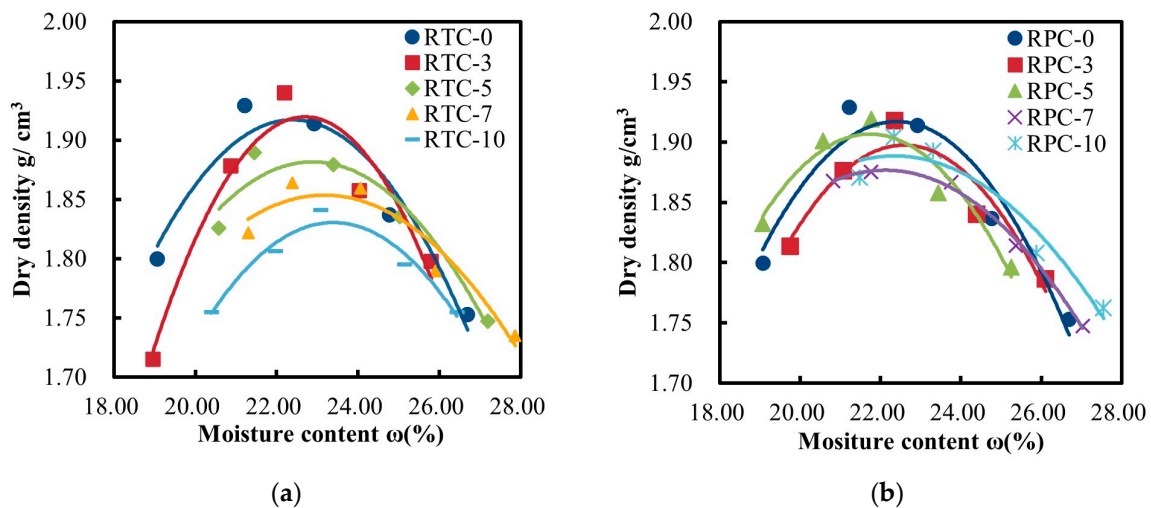| Number	Maximum Dry Density (g/cm^3)	Optimum Moisture Content/%	Number	Maximum Dry Density (g/cm^3)	Optimum Moisture Content/%
RTC-0	1.92	22.39	RPC-0	1.92	22.39
RTC-3	1.91	22.66	RPC-3	1.90	22.59
RTC-5	1.89	22.92	RPC-5	1.93	21.85
RTC-7	1.84	23.10	RPC-7	1.89	22.26
RTC-10	1.81	23.26	RPC-10	1.88	22.24

(a)

(b)

Figure 3. Compaction curves of samples with different gypsum and mix ratios. (**a**) RTC compaction curves with different mix ratios; (**b**) RPC compaction curves with different mix ratios.

3.2. Unconfined Compressive Strength Analysis

3.2.1. RTC Unconfined Compressive Strength Analysis

The results of the unconfined compressive strength tests of the RTC specimens are shown in Figure 4. The compressive strength of the RTC increased with increasing additions of titanium gypsum. When the titanium gypsum admixture was 0 wt%, there was no significant increase in the strength of the composites from 7 d to 28 d, and a decrease in strength was observed at 14 d. And, when the titanium gypsum admixture was 10 wt%, the 7 d strength reached 8.8 MPa, and the 28 d strength was able to reach 11.8 MPa. This indicates that the addition of titanium gypsum produces free Ca^{2+}, SO_4^{2-} in the mixture. The water in the red mud contained a large amount of OH^-, which can react with SiO_2 and Al_2O_3 in the red mud to generate reaction products such as calcium silicate hydrated, calcium aluminate hydrated, or calcium sulfoaluminate hydrated. It also wraps the red mud agglomerates with cement hydration products to form a more stable cemented whole [33]. The addition of titanium gypsum and cement caused the red mud-based composites to form a reticulated and stabilized structure with a combination of cementitious and crystalline associations through the processes of cement hydration and alkali excitation [34].
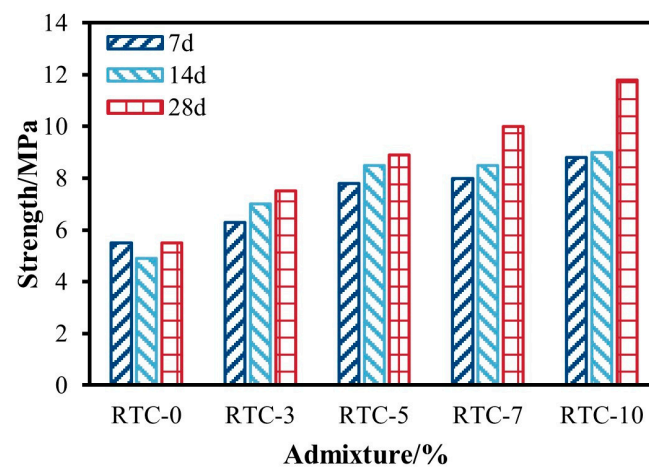

Figure 4. RTC unconfined compressive strength.

The ages of curing of the specimens immersed in water were 7 d (6 d in the curing room, 1 d in the immersion), 14 d (13 d in the curing room, 1 d in the immersion), and

28 d (27 d in the curing room, 1 d in the immersion) [35]. The unconfined compressive strength of the RTC after immersion is shown in Figure 5. A comparison of the unconfined compressive strength of the RTC after 7 d and 28 d of immersion was used to analyze the influence of the soaked conditions on the strength of the red mud-based composites. The results are shown in Figure 6.
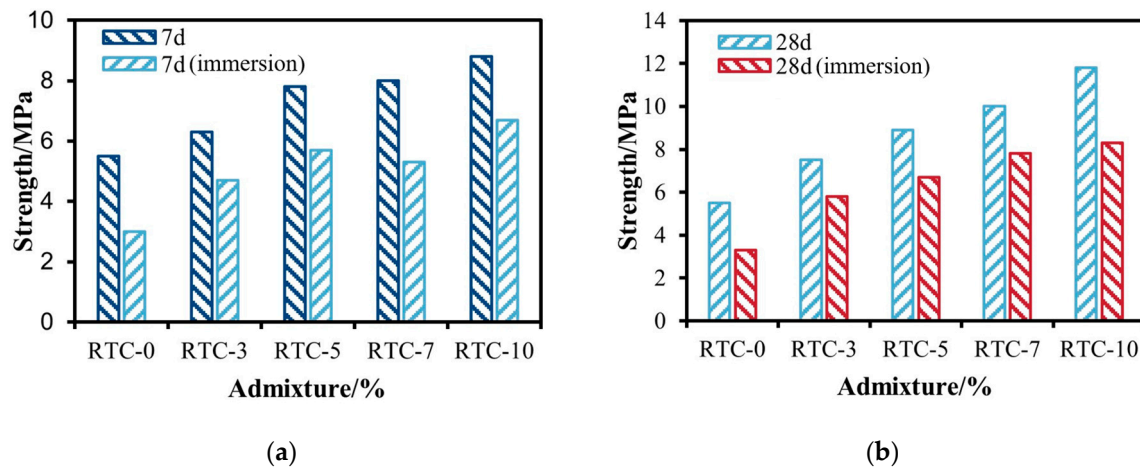

(**a**)   (**b**)

Figure 5. Unconfined compressive strength after 7 d and 28 d of RTC curing. (**a**) Unconfined compressive strength after 7 d of RTC curing; (**b**) unconfined compressive strength after 28 d of RTC curing.
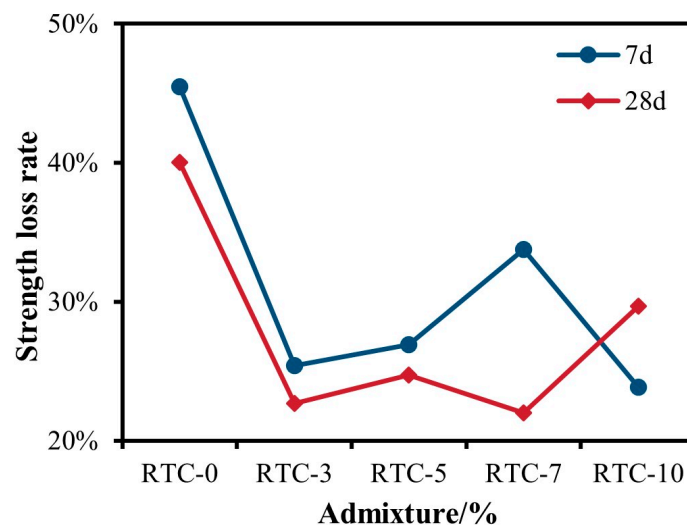
Figure 6. Rate of strength loss of RTC after immersion.

It can be found from the test results that when only cement was used to treat the red mud, the strength of the modified red mud was lost more after immersion, and the overall water stability was poor. The loss of strength reached 45% at 7 d and 40% at 28 d. In contrast, the red mud-based composites with added titanium gypsum had a relatively small loss of strength after immersion. The smallest loss was RTC-7, which was for 28 d, with a loss of 22%.

3.2.2. RPC Unconfined Compressive Strength Analysis

The results of the RPC unconfined compressive strength tests are shown in Figure 7. The admixture of phosphogypsum in the RPC had a significant effect on its strength. The strength of the modified red mud first increased and then decreased with phosphogypsum addition. The RPC-5 had the largest increase in unconfined compressive strength at 28 d,

with a 125.5% increase in the 28 d strength compared to RPC-0. The modified red mud specimen with the 5 wt% phosphogypsum admixture had a maximum strength of 12.4 MPa at 28 d. This is because the Ca^{2+} and SO_4^{2-} dissolved in phosphogypsum accelerate the chemical reaction to produce a large number of ettringite with swelling properties. Ettringite fills the pores, and the mutual cross-linking between needle crystals binds many of the particles together to form a spatial structure along with hydrated calcium silicate and hydrated calcium silicate [36], which makes the structure denser and thus improves the strength of the RPC.
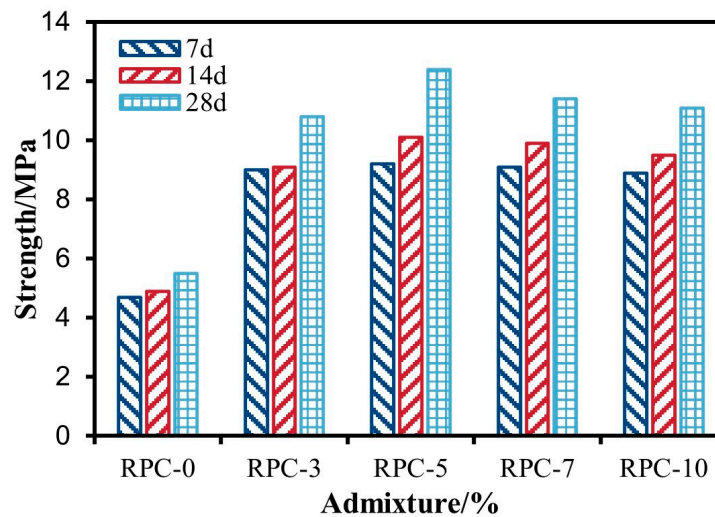
Figure 7. RPC unconfined compressive strength.

The immersion conditions for RPC were the same as those for RTC. The unconfined compressive strength of RPC after immersion is shown in Figure 8. A comparison of the unconfined compressive strength of RPC after 7 d and 28 d of immersion was used to analyze the influence of the soaked conditions on the strength of the red mud-based composites. The results are shown in Figure 9.
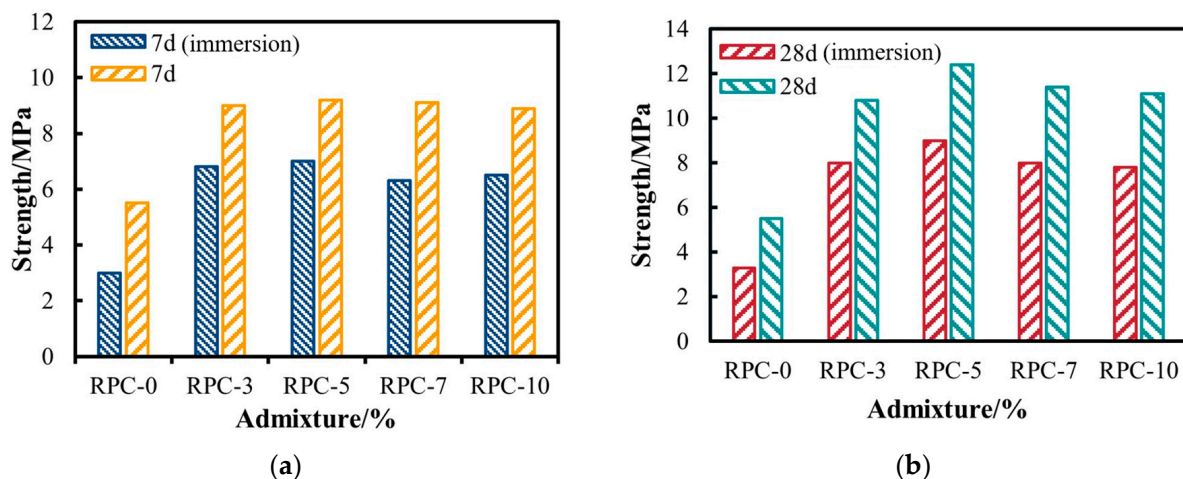

Figure 8. Unconfined compressive strength after 7 d and 28 d of RPC curing. (**a**) Unconfined compressive strength after 7 d of RPC curing; (**b**) unconfined compressive strength after 28 d of RPC curing.
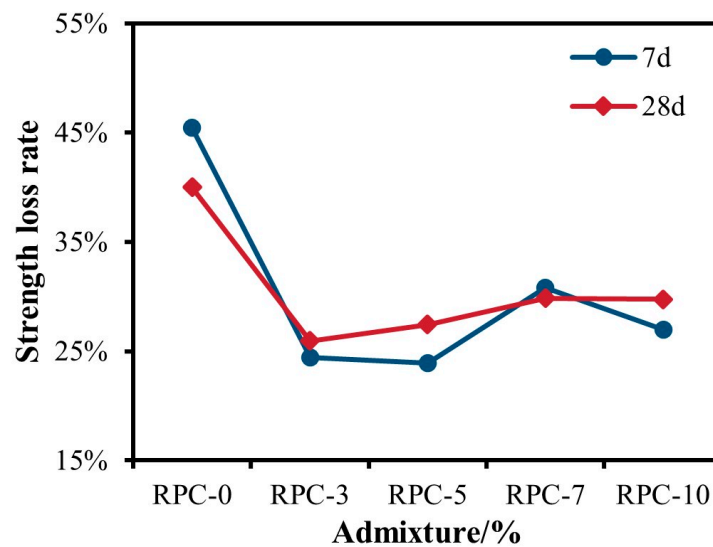
Figure 9. Rate of strength loss of RPC after immersion.

As can be seen from the figure, compared to RPC-0, the red mud-based composites with added phosphogypsum had a relatively small loss of strength after immersion. The smallest loss was RPC-5, which was for 7 d, with a loss of 24%.

3.2.3. Comparative Analysis of RTC and RPC Unconfined Compressive Strength

Figure 10 shows the variation curves of the unconfined compressive strength with the gypsum admixture after 7 d and 28 d for the modified red mud composites. The figure shows that the RTC 7 d and 28 d strengths increased. Figure 10a shows that the unconfined compressive strength of the RC was about 5.5 MPa after 7 d of curing, and the strength of the samples increased by 14.5%, 41.8%, 45.5%, and 61.6% as the titanium gypsum admixture was elevated to 3%, 5%, 7%, and 10%, respectively. When the phosphogypsum admixture was not more than 3%, the RPC strength increased significantly with the admixture, and the strength reached up to 9 MPa. The RPC strength changed slowly when the phosphogypsum admixture was more than 3%. Figure 10b shows that the RTC strength grew with the increases in the titanium gypsum admixture and reached 11.8 MPa when the admixture reached 10%, which was an increase of 114.5% compared to the RC strength. The RPC strength showed an increasing and then decreasing trend with the increase in phosphogypsum admixture, and the strength reached a maximum of 12.4 MPa when the phosphogypsum admixture was 5%, which was an increase of 125.5% compared to the RC strength. Based on the unconfined compressive strength after 7 d and 28 d, the strength of the phosphogypsum was higher than that of the titanium gypsum at the same admixture and same age, and the strength of the titanium gypsum-modified red mud exhibited an upward trend. However, when the gypsum admixture was controlled to be less than 10%, the RPC was superior to the RTC. This was due to the addition of gypsum, which promoted the hydration reaction within the matrix, generating a large number of ettringite (AFt) with calcium silicate hydrate (C-S-H) cross-growth, forming a dense net structure, and refining the internal pore size of the matrix [31]. It can be seen that the modified red mud composite with the best strength was RPC-5. The truss structure in the building was also formed in the RPC compared to the RTC, resulting in a higher strength of the specimen. This was consistent with the results of the microstructure analysis of the specimen.
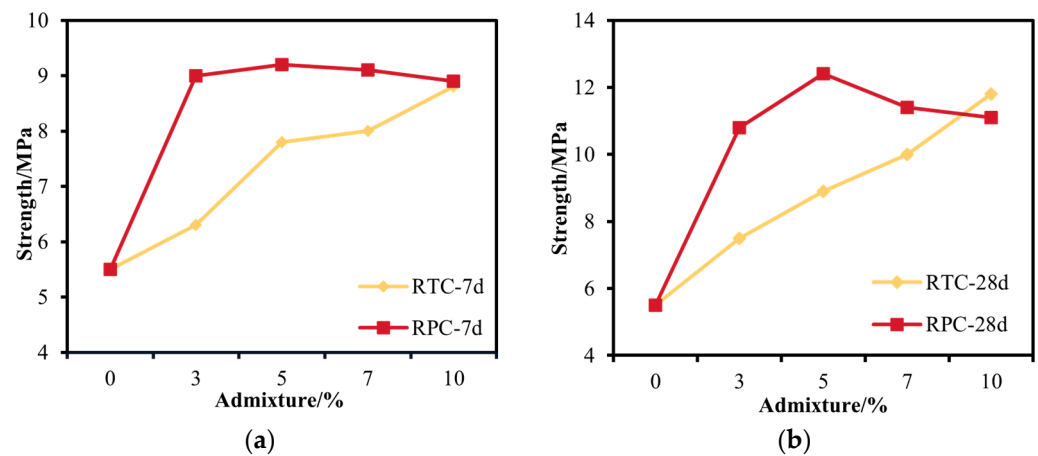
Figure 10. Variation curve of unconfined compressive strength of specimens with different gypsum admixtures. (**a**) Change curve of 7 d compressive strength with gypsum admixture; (**b**) change curve of 28 d compressive strength with gypsum admixture.

3.3. Microstructure Analysis

3.3.1. Comparative Analysis of RC and RTC Microstructures

Figure 11 shows the SEM micrographs of the specimen sections of RC specimens magnified by 2000 and 8000 times after 28 d of curing, respectively. The microstructures of the hydration products of the RC specimens at the age of 28 d consisted of part of a fine acicular material and amorphous gel, forming a spatial reticulation of the combination of colloidal–crystalline materials. However, the structure had more cracks and a certain number of unfilled pores. The fine acicular material was ettringite (AFt), and the amorphous gel was a calcium silicate hydrate (C-S-H). The C-S-H structure connected some fine particles, and the generation of these substances was the basis for the early strength development of the filling body. The overall structure of the filled body was denser, so the early strength was relatively high. With the increase in the age of curing, the hydration reaction of the cement continued, the activity of the red mud was stimulated, a small amount of AFt and a large amount of C-S-H were generated, and the crystals gradually developed [37].
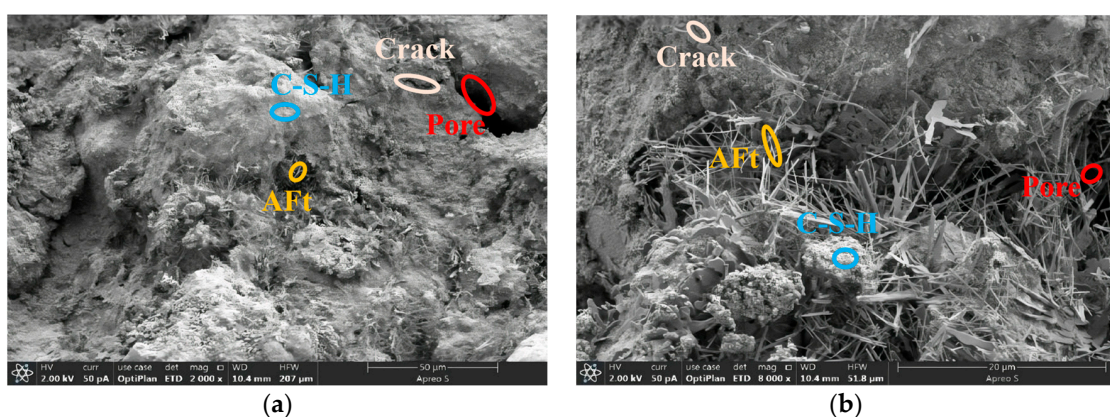

Figure 11. SEM micrographs of RC at different magnifications. (**a**) SEM micrograph of RC specimen section at 2000×; (**b**) SEM micrograph of RC specimen section at 8000×.

Figure 12 shows the SEM micrographs of RTC specimens added with 5% titanium gypsum at a magnification of 2000 times and 8000 times after 28 d of curing. It can be seen that, with the addition of titanium gypsum, more particles with more complex shapes and different sizes appeared, and voids still existed between the particles. But compared with the specimens without titanium gypsum, the pores of the RTC-5 specimens became

smaller at the age of 28 d, the number of cracks decreased, and finer acicular material AFt appeared. The fine acicular materials began to interweave with each other, the C-S-H gelation increased gradually, and the pores inside the specimens were gradually filled by the hydration products, which laid a structural foundation for enhancing the specimen's mechanical strength.
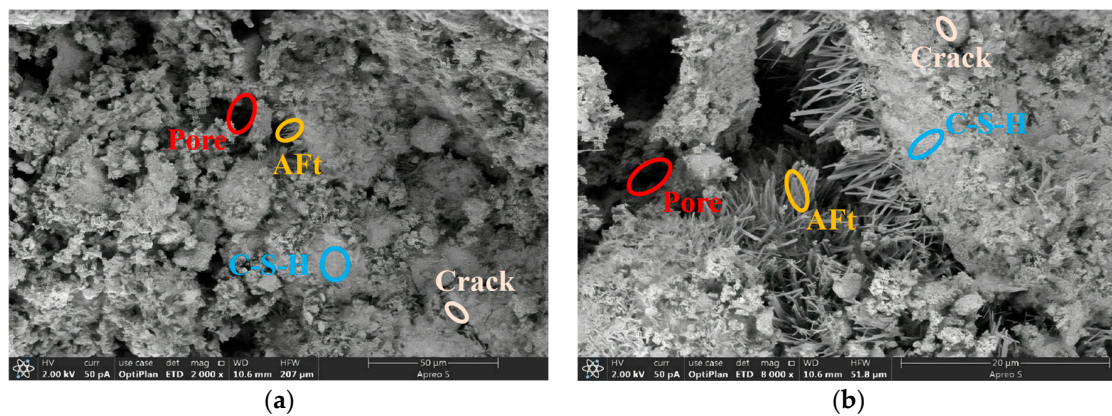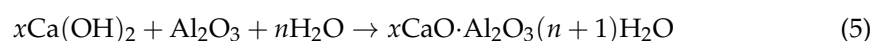

(a) (b)

Figure 12. SEM micrographs of RTC-5 at different magnifications. (**a**) SEM micrograph of RTC-5 specimen section at 2000×; (**b**) SEM micrograph of RTC-5 specimen section at 8000×.

Figure 13 shows the SEM micrographs of sections of the RTC specimens added with 10% titanium gypsum at magnifications of 2000 and 8000 times after 28 d of curing, respectively. As the admixture of titanium gypsum continued to increase, a coarser and wider AFt columnar structure was produced inside the matrix. The internal structure of the filled body was covered by a large amount of reticulated C-S-H, which further reduced the number of internal pores and cracks. This resulted in a dense structure, better integrity, and increased strength. This is because the addition of titanium gypsum produced a large number of free Ca^{2+} and SO_4^{2-}, and the water in the red mud contained a large number of OH^-, which could react chemically with the SiO_2 and Al_2O_3 in the red mud to generate reaction products such as calcium silicate hydrated, calcium aluminate hydrated, or calcium thioaluminate hydrated. This is the mechanism of action of the calcium-based material curing of the red mud-based composites. The reactions are as follows [33]:

$$x\mathrm{Ca(OH)_2} + \mathrm{SiO_2} + n\mathrm{H_2O} \rightarrow x\mathrm{CaO \cdot SiO_2}(n+1)\mathrm{H_2O} \tag{4}$$

$$x\mathrm{Ca(OH)_2} + \mathrm{Al_2O_3} + n\mathrm{H_2O} \rightarrow x\mathrm{CaO \cdot Al_2O_3}(n+1)\mathrm{H_2O} \tag{5}$$

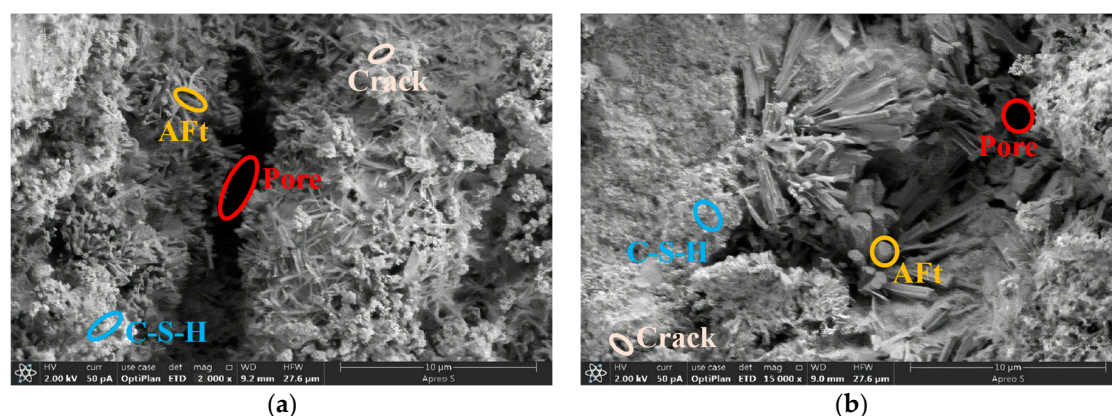This is also consistent with the strength test results.

(a) (b)

Figure 13. SEM micrographs of RTC-10 at different magnifications. (**a**) SEM micrograph of RTC-10 specimen section at 2000×; (**b**) SEM micrograph of RTC-10 specimen section at 15,000×.

3.3.2. RPC Microstructure Analysis

Figure 14 shows the SEM micrographs of sections of the RPC specimens with the 3% phosphogypsum admixture at magnifications of 4000 and 15,000 times after 28 d of curing, respectively. The figure shows that a large number of hedgehog-like crystals AFt appeared in the composites with 3% phosphogypsum added, while lumps were visible in the clusters of AFt crystals. The structures were gradually linked into a dense whole with fewer cracks under the connection of AFt. The addition of phosphogypsum produced free Ca^{2+} and SO_4^{2-} ions in the composite material, while the moisture in the red mud contained a large amount of OH^-. With the increased pH in the moisture, they reacted chemically with the SiO_2 and Al_2O_3 in the red mud to generate reaction products such as calcium silicate hydrated, calcium aluminate hydrated, or calcium sulphoaluminate hydrated under the joint action. Together with the cement hydration products, they wrapped red mud aggregates, forming a more stable cemented whole [33].
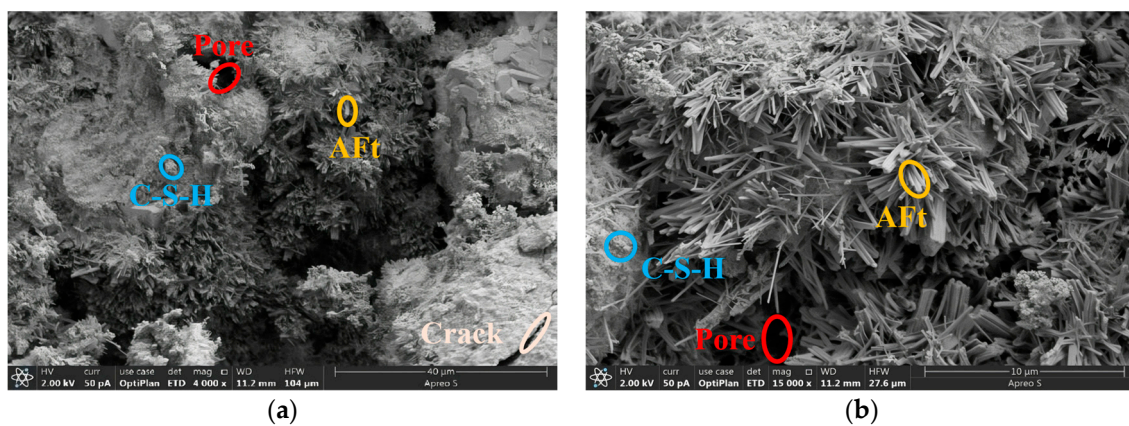

Figure 14. SEM micrographs of RPC-3 at different magnifications. (**a**) SEM micrograph of RPC-3 specimen section at 4000×; (**b**) SEM micrograph of RPC-3 specimen section at 15,000×.

Figure 15 shows the SEM micrographs of specimen sections of tbe RPC specimens with the 5% phosphogypsum admixture at magnifications of 4000 and 15,000 times after 28 d of curing. As can be seen from the figure, the increase in the phosphogypsum admixture to 5% further promoted the hydration reaction between the gelling material and the active substances in the red mud. A large amount of AFt and C-S-H grew interlaced and are tightly wrapped by the gel, forming a dense net structure, effectively refining the internal pore size and cracks of the matrix, and forming a truss structure like in the building, thus increasing the strength of the specimen. RPC-5 underwent cement hydration reaction and alkali excitation to form a stable mesh structure with a combination of cementitious and crystalline associations [31].

Figure 16 shows the SEM micrographs of specimen sections of RPC specimens with the 10% phosphogypsum admixture at magnifications of 4000 and 15,000 times after 28 d of curing. As can be seen from the figure, when the phosphogypsum admixture was increased to 10%, the pore size of the specimens increased, the number of cracks increased, and C-S-H did not form a mesh structure, which indicates that the addition of excess phosphogypsum affected the strength of the composites. This is because the mineral composition based on the Bayer method of the red mud was mainly silicoaluminate. As the reaction proceeded, a large amount of OH^- was dissolved. When the pH value rose to a certain level, the Ca^{2+} in the solution reacted chemically with active Si and Al_2O_3 to generate calcareous alumina, katenite, etc., and the Ca^{2+} concentration was gradually reduced. The concentrations of SiO_4^{4-} and AlO^{2-} were due to the continuous depolymerization of the alumina–silicates in the raw material, which gradually increased, inhibiting the generation of AFt [38]. This corresponds to the results of the unconfined compressive strength tests.
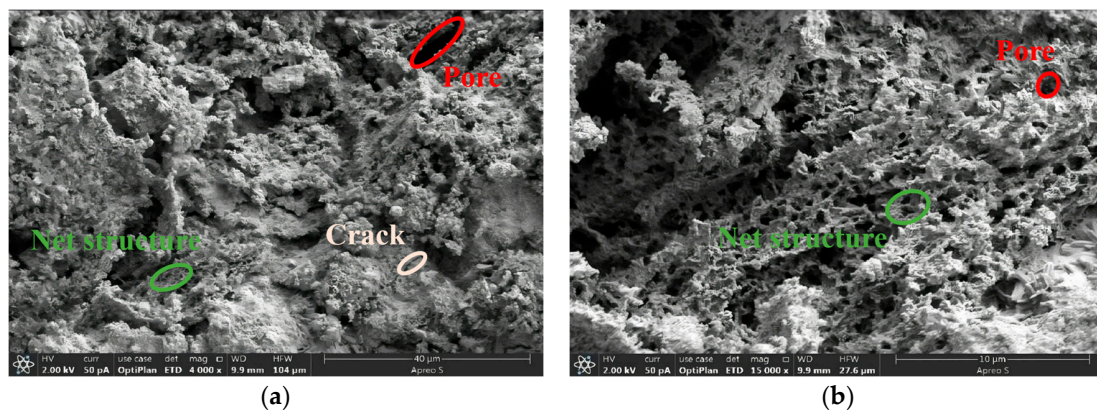
Figure 15. SEM micrographs of RPC-5 at different magnifications. (**a**) SEM micrograph of RPC-5 specimen section at 4000×; (**b**) SEM micrograph of RPC-5 specimen section at 15,000×.
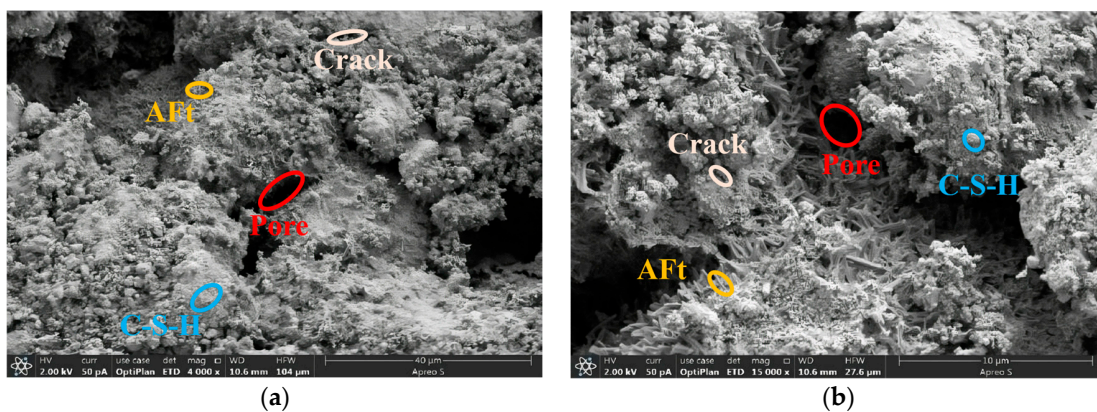

Figure 16. SEM micrographs of RPC-10 at different magnifications. (**a**) SEM micrograph of RPC-10 specimen section at 4000×; (**b**) SEM micrograph of RPC-10 specimen section at 15,000×.

3.4. Analysis of Heavy Metal Leaching Pattern

The results of the continuous flume leaching test after eight cycles are shown in Table 10 and Figure 17. The cumulative releases of the heavy metals As, Mo, Zn, and Cr were all larger, while the cumulative releases of Pb, Se, Ba, and Cu were smaller. However, the inhibition effects of phosphogypsum on As, Mo, and Cr leaching were better than that of the titanium gypsum, and the inhibition effects on Zn leaching were weaker than that of the titanium gypsum. When the gypsum admixture was the same at 5%, the cumulative release of As, Mo, and Cr in the RPC was 0.01655 mg/L, 0.02559 mg/L, and 0.00762 mg/L lower than that of RTC, respectively, and the cumulative release of Zn was 0.00719 mg/L higher than that of RTC. When the gypsum admixture was the same at 10%, the cumulative release of As, Mo, and Cr in the RPC was lower than that of RTC by 0.01078 mg/L, 0.05193 mg/L, and 0.01521 mg/L, respectively, and the cumulative release of Zn was higher than that of RTC by 0.01336 mg/L. The cumulative release of heavy metal elements through leaching in the RTC and RPC was found to meet the discharge standards for Class III groundwater. This is because the addition of titanium gypsum and phosphogypsum generates AFt, which is capable of interconnecting and filling the internal structure of the material so that the heavy metal elements in the material are encapsulated in the modified material in the form of complexes due to precipitation or other means [39]. However, there are long-term leaching behaviors of heavy metal elements in composites, such as Ni, Cr, Ba, As, Se, Zn, etc. The leaching behaviors of heavy metal elements can still be detected after several leaching cycles. This is because in the long-term leaching process, the gel structure is slowly eroded, and the heavy metal elements in the material diffuse into the leaching solution through the pore water. In contrast, the collodion minerals or nascent hydration products

in the uneroded portion continue to encapsulate or adsorb the heavy metal elements, which continue to be present in the matrix and are not fully released [31]. This indicates that when the modified red mud material is applied to road sub-base materials, it is necessary to carry out a long-term test on the release of heavy metals to avoid the excessive release of heavy metals leading to environmental pollution.

Table 10. Results of continuous flume leaching tests.

|	Group III Groundwater	RC	RTC-5	RTC-10	RPC-5	RPC-10
Be (mg/L)	≤0.0002	—	—	—	—	—
Cr (mg/L)	≤0.05	0.014419	0.02709	0.02572	0.01947	0.01051
Mn (mg/L)	≤0.1	0.00158	0.00014	—	—	—
Co (mg/L)	≤0.05	0.00020	0.00002	0.00003	0.00002	—
Ni (mg/L)	≤0.05	0.00034	0.00015	0.00039	0.00169	—
Cu (mg/L)	≤1.0	0.00273	0.00004	0.00085	0.00080	0.00044
Zn (mg/L)	≤1.0	0.02643	0.01017	0.0052	0.01736	0.01856
As (mg/L)	≤0.05	0.09978	0.04719	0.02151	0.03064	0.01073
Se (mg/L)	≤0.01	0.00078	0.00132	0.00141	0.00129	0.00133
Mo (mg/L)	≤0.1	0.05653	0.08971	0.08766	0.06412	0.03573
Cd (mg/L)	≤0.01	0.00013	—	—	—	—
Ba (mg/L)	≤1.0	0.00271	0.00144	0.00199	0.00204	0.00428
Hg (mg/L)	≤0.001	—	—	—	—	—
Pb (mg/L)	≤0.05	0.00767	—	0.00046	0.00013	0.00026
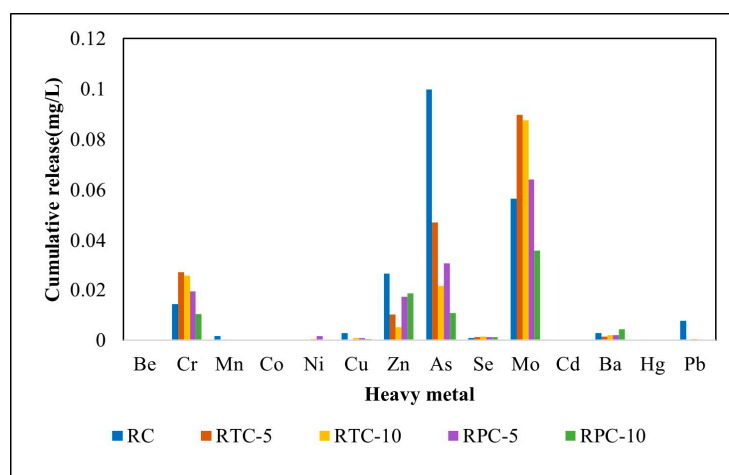
Figure 17. Cumulative heavy metal release results. Based on the above experimental results, the cumulative release pattern of the heavy metals As, Mo, and Ba from the modified red mud composites was analyzed.

3.4.1. Analysis of the Leaching Pattern of As

Figure 18 shows the cumulative release of As in the specimens with time and dosage for different gypsum admixtures. Based on the figure, the cumulative release of As reaches a steady state after the leaching time reaches 16 d. With the increase in titanium gypsum and phosphogypsum dosing, the total cumulative release of As exhibits a decreasing trend. For the same 5% admixture of titanium gypsum and phosphogypsum, the total leaching of As in the composites was 8.14 mg/m^2 and 5.07 mg/m^2, respectively, which was 8.88 mg/m^2 and 11.95 mg/m^2 less than that of the specimens without gypsum addition. For the same 10% admixture of titanium gypsum and phosphogypsum, the total leaching of As in the composites was 3.73 mg/m^2 and 1.82 mg/m^2, respectively, which was 13.29 mg/m^2 and 15.2 mg/m^2 less than that of the specimens without gypsum addition. It can be seen that phosphogypsum inhibits the leaching of As better than titanium gypsum with the same amount of gypsum admixture.
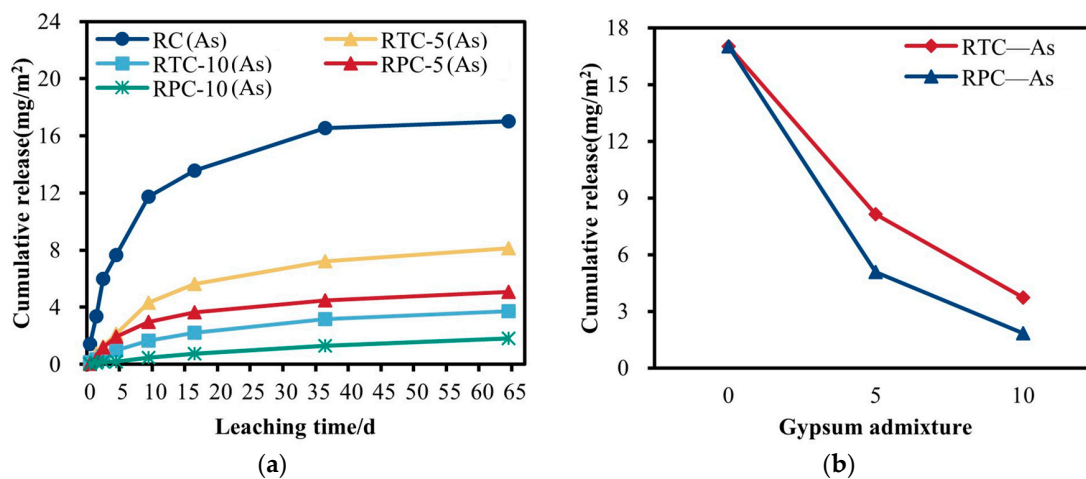
Figure 18. Variation curves of cumulative release of As with time and dosage in specimens with different gypsum admixtures. (**a**) Variations in the cumulative release of As with time; (**b**) variations in the cumulative release of As with admixture.

3.4.2. Analysis of the Leaching Pattern of Mo

Figure 19 shows the cumulative release of Mo in the specimens with time and dosage for different gypsum admixtures. Based on the figure, the cumulative release of Mo entered a slow growth phase after the leaching time reached 16 d. With increasing titanium gypsum and phosphogypsum incorporation, the overall total cumulative release of Mo both showed an increasing trend followed by a decreasing trend, but with differences. For the same 5% admixture of titanium gypsum and phosphogypsum, the total leaching of Mo in the composites was 15.74 mg/m^2 and 10.61 mg/m^2, respectively. The composites with titanium gypsum had a higher total amount of leaching than the composites with phosphogypsum by 5.13 mg/m^2. At the same 10% admixture of titanium gypsum and phosphogypsum, the total leaching of Mo in the composites was 15.20 mg/m^2 and 6.06 mg/m^2, respectively. The composites with titanium gypsum had a higher total amount of leaching than the composites with phosphogypsum by 9.14 mg/m^2. At the same dosage of 5%, both the titanium gypsum and phosphogypsum promoted the leaching of Mo in the composites. At the same dosage of 10%, the addition of titanium gypsum still promoted the leaching of Mo in the composites, while the addition of phosphogypsum inhibited the leaching of Mo in the composites.
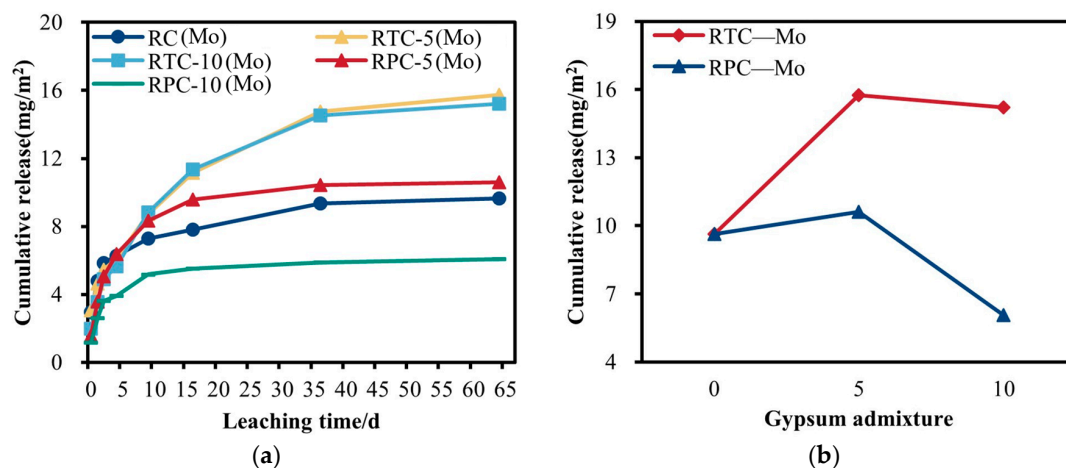

Figure 19. Variation curves of cumulative release of Mo with time and dosage in specimens with different gypsum admixtures. (**a**) Variations in the cumulative release of Mo with time; (**b**) variation in the cumulative release of Mo with admixture.

3.4.3. Analysis of the Leaching Pattern of Ba

Figure 20 shows the cumulative release of Ba in the specimens with time and dosage for different gypsum admixtures. Based on the figure, the cumulative release of Ba entered a slow growth phase after the leaching time reached 16 d. With increasing titanium gypsum and phosphogypsum incorporation, the overall total cumulative release of Ba both showed a decreasing trend followed by an increasing trend, but with differences. For the same 5% admixture of titanium gypsum and phosphogypsum, the total leaching of Ba in the composites was 0.25 mg/m^2 and 0.34 mg/m^2, respectively. The composites with titanium gypsum had a lower total amount of leaching than the composites with phosphogypsum by 0.09 mg/m^2. At the same, for the 10% admixture of titanium gypsum and phosphogypsum, the total leaching of Ba in the composites was 0.34 mg/m^2 and 0.73 mg/m^2, respectively. The composites with titanium gypsum had a lower total amount of leaching than the composites with phosphogypsum by 0.39 mg/m^2. At the same dosage of 5%, both titanium gypsum and phosphogypsum inhibited the leaching of Ba in the composites. At the same dosage of 10%, the addition of titanium gypsum still inhibited the leaching of Mo in the composites, while the addition of phosphogypsum promoted the leaching of Mo in the composites.
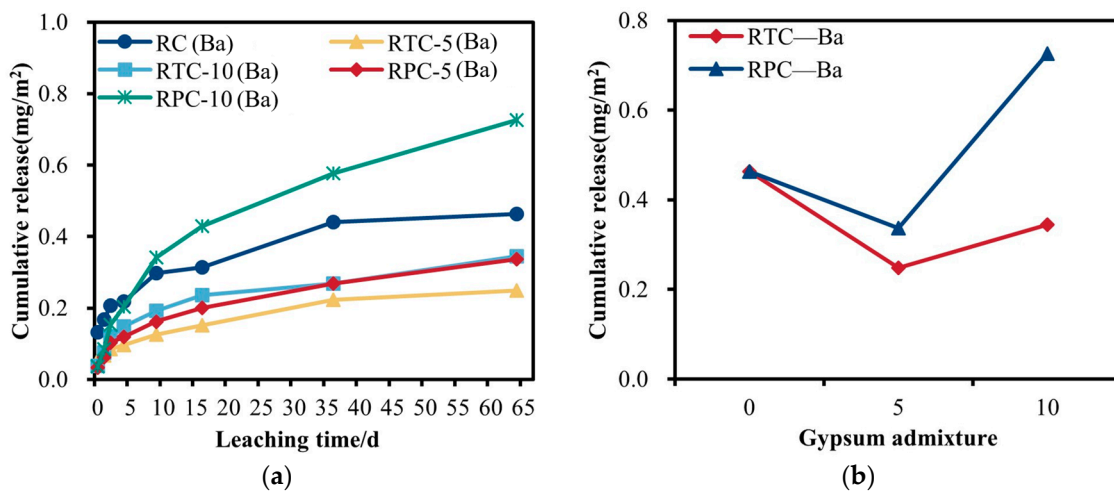

Figure 20. Variation curves of cumulative release of Ba with time and dosage in specimens with different gypsum admixtures. (**a**) Variations in the cumulative release of Ba with time; (**b**) variations in the cumulative release of Ba with admixture.

4. Conclusions and Prospects

4.1. Conclusions

In this paper, the compaction characteristics, unconfined compressive strength, microstructure, and heavy metal leaching patterns of RTC and RPC with different gypsum admixtures were investigated, and the optimal ratio of gypsum–cement-stabilized red mud composites was selected. The main conclusions are as follows:

(1) The results of the compaction test showed that there were minor differences in the optimal moisture content between RTC and RPC, while the maximum dry densities of the two were very close to each other, at 1.91 g/cm³ and 1.93 g/cm³, respectively.

(2) Based on the unconfined compressive strength at 7 d and 28 d, when the admixture of gypsum was controlled to be less than 10%, the RPC was better than the RTC. When the phosphogypsum admixture was 5%, the strength reached a maximum of 12.4 MPa. RPC-5 showed a 125.5% increase in strength compared to RC.

(3) Based on the 28 d microstructure of the specimens, phosphogypsum cured better at the optimum mixing ratio. Among them, RPC-5 had the best curing effect, with a denser structure with fewer pores.

(4) The cumulative releases of As, Mo, Zn, and Cr from the 8% cement-stabilized red mud material in the continuous flume leaching experiments were larger. The cumulative releases were 0.09978 mg/L, 0.05653 mg/L, 0.02643 mg/L, and 0.014419 mg/L, respectively. The two gypsum additions had the same effect on the leaching of the As and different effects on the leaching of Mo and Ba.

(5) Summarizing all the test results, the optimal modified red mud material that met both the mechanical requirements of road subgrade materials and the requirements of groundwater standards was the RPC, and the optimal mix ratio was red mud/phosphogypsum/cement = 87:5:8.

4.2. Prospects and Limitations

(1) In this paper, only the effects of two gypsums on the mechanical properties and heavy metal leaching of red mud-based composites were investigated when the cement was 8%. The effects of the two gypsums on the composites were not investigated when the cement dosage was less than 8% or more than 8%. In addition, only 96% compaction was used to prepare the specimens in this paper. The effects of other compaction levels on the material performance characteristics were not investigated.

(2) The research in this paper only carried out indoor tests, and no work was carried out on the experimental sections of the modified red mud. The large-scale application of modified red mud for road construction requires long-term stability testing of gypsum–cement-stabilized composites. The results of the heavy metal leaching tests likewise indicate the need to analyze groundwater and soil hazards through long-term monitoring of the cumulative releases of heavy metals from the materials.

References

1. Editorial Board of the Dictionary of Environmental Science. *Dictionary of Environmental Science*, 2nd ed.; China Environmental Science Press: Beijing, China, 2008; pp. 60–61.
2. Zhang, Y.; Wang, Y.; Wang, K.; Dou, Z.; Liu, Y.; Zhao, Q.; Niu, L.; Zhang, Z.; Han, J.; Guo, J. A Method of Iron Extraction and Direct Cementation of High Iron Red Mud. China Patent No. 201910291219.4, 12 October 2021.
3. Liang, G.; Chen, W.; Nguyen, A.; Nguyen, T. Red mud carbonation using carbon dioxide: Effects of carbonate and calcium ions on goethite surface properties and settling. *J. Colloid Interface Sci.* **2018**, *517*, 230–238. [CrossRef] [PubMed]
4. Khairul, M.; Zanganeh, J.; Moghtaderi, B. The composition, recycling and utilisation of Bayer red mud. *Resour. Conserv. Recycl.* **2019**, *141*, 483–498. [CrossRef]
5. Wang, Y. Strength Characteristics and Micro-Mechanism of Red Mud-Based Modified Silt Loam. Master's Thesis, Zhongyuan University of Technology, Zhengzhou, China, 2022.
6. Xie, W.; Zhang, N.; Li, J.; Zhou, F.; Ma, X.; Gu, G.; Zhang, W. Optimization of condition for extraction of aluminum and iron from red mud by hydrochloric acid leaching. *Chin. J. Environ. Eng.* **2017**, *11*, 5677–5682. [CrossRef]
7. Ning, L.; He, D.; Chen, W.; Zhou, K.; Peng, C.; Zhang, X.; Teng, C. Sulfuric Acid Leaching and Kinetics Study for Separation of Iron and Scandium from Red Mud. *Min. Metall. Eng.* **2019**, *39*, 81–84+88. [CrossRef]
8. Luo, S.; Liu, M.; Yang, L.; Chang, J.; Yang, W.; Yan, X.; Yu, H.; Shen, Y. Utilization of waste from alumina industry to produce sustainable cement-based materials. *Constr. Build. Mater.* **2019**, *229*, 116795. [CrossRef]

9. Bai, B.; Bai, F.; Li, X.; Nie, Q.; Jia, X.; Wu, H. The remediation efficiency of heavy metal pollutants in water by industrial red mud particle waste. *Environ. Technol. Innov.* **2022**, *28*, 102944. [CrossRef]

10. Xie, J.; He, B.; Chen, T.; Zhang, N.; Peng, X.; Nie, X.; Ma, F. Characterization of red mud and fly ash based for co-curing of Cu^{2+}-contaminated soil. *Case Stud. Constr. Mater.* **2024**, *20*, e02769. [CrossRef]

11. Santona, L.; Castaldi, P.; Melis, P. Evaluation of the interaction mechanisms between red muds and heavy metals. *J. Hazard. Mater.* **2006**, *136*, 324–329. [CrossRef] [PubMed]

12. Liang, Z.; Peng, X.; Luan, Z. Immobilization of Cd, Zn and Pb in sewage sludge using red mud. *Environ. Earth Sci.* **2012**, *66*, 1321–1328. [CrossRef]

13. Sutar, H.; Mishra, S.C.; Sahoo, S.K.; Chakraverty, A.P.; Maharana, H.S. Progress of Red Mud Utilization: An Overview. *Am. Chem. Sci. J.* **2014**, *4*, 255–279. [CrossRef]

14. Sarath Chandra, K.; Krishnaiah, S. Strength and leaching characteristics of red mud (bauxite residue) as a geomaterial in synergy with fly ash and gypsum. *Transp. Res. Interdiscip. Perspect.* **2022**, *13*, 100566. [CrossRef]

15. Li, H.; Yang, Y.; Wang, X.; Tang, H. Effects of the position and chloride-induced corrosion of strand on bonding behavior between the steel strand and concrete. *Structures* **2023**, *58*, 105500. [CrossRef]

16. Zhang, M.; Wu, Y.; Li, Y.; Zhou, R.; Yu, H.; Zhu, X.; Quan, H.; Li, Y. Risk assessment for the long-term stability of fly ash-based cementitious material containing arsenic: Dynamic and semidynamic leaching. *Environ. Pollut.* **2024**, *345*, 123361. [CrossRef]

17. Li, Z.; Gao, M.; Lei, Z.; Tong, L.; Sun, J.; Wang, Y.; Wang, X.; Jiang, X. Ternary cementless composite based on red mud, ultra-fine fly ash, and GGBS: Synergistic utilization and geopolymerization mechanism. *Case Stud. Constr. Mater.* **2023**, *19 Pt A*, e02410. [CrossRef]

18. Deelwal, K. Evaluation of characteristic properties of red mud for possible use as a geotechnical material in civil construction. *Int. J. Adv. Eng. Technol.* **2014**, *7*, 1053–1059.

19. Shi, M.; Tian, X.; Wang, H.; Yu, C.; Du, X.; Zhang, R. Performance of Cement-Lime-Phosphogypsum Solidified Red Mud as Road Base Material. *J. Changjiang River Sci. Res. Inst.* **2024**, *41*, 114–120. [CrossRef]

20. Yu, C. Feasibility Study on Phosphogypsum Modified Cement-Lime Stabilized Red Cement Road Base Material. Master's Thesis, Southeast University, Nanjing, China, 2021.

21. Li, C. Study on the Basic Performance and Engineering Application of Bayer Red Mud Used in Roadbed Filling Applications. Master's Thesis, Shandong Jianzhu University, Jinan, China, 2018.

22. Zeng, H.; Jin, M.; Li, W.; Gao, C.; Ma, Y.; Guan, Q.; Liu, J. Performance evolution of low heat cement under thermal cycling fatigue: A comparative study with moderate heat cement and ordinary Portland cement. *Constr. Build. Mater.* **2024**, *412*, 134863. [CrossRef]

23. Pu, S.; Zhu, Z.; Huo, W. Evaluation of engineering properties and environmental effect of recycled gypsum stabilized soil in geotechnical engineering: A comprehensive review. *Resour. Conserv. Recycl.* **2021**, *174*, 105780. [CrossRef]

24. Li, Z.; Zhang, J.; Li, S.; Gao, Y.; Liu, C.; Qi, Y. Effect of different gypsums on the workability and mechanical properties of red mud-slag based grouting materials. *J. Clean. Prod.* **2020**, *245*, 118759. [CrossRef]

25. Suo, C.; Wen, H.; Cao, J.; Dong, X. Performance of a Composite Soil Prepared with Red Mud and Desulfurized Gypsum. *Ksce J. Civ. Eng.* **2022**, *26*, 47–56. [CrossRef]

26. Zhang, S.; Ding, J.; Lai, Z.; Guo, Q.; Wan, X. Mechanical and microstructural properties of silt roadbed filling improved with cement, red mud and desulfurization gypsum. *Eur. J. Environ. Civ. Eng.* **2024**, *28*, 176–196. [CrossRef]

27. Zhang, J.; Yan, G.; Bai, X.; Kong, S.; Li, J.; Li, G.; Ge, Z.; Huang, J. Resource Utilization Potential of Red Mud: A Study on the Micro-Mechanism of the Synergistic Effect of Multiple Solid Waste Filling Materials. *Sustainability* **2023**, *15*, 15532. [CrossRef]

28. *GB/T 14848-2017*; Standard for Groundwater Quality. 2nd ed. Standards Press of China: Beijing, China, 2017.

29. *JTG 3430-2020*; Test Methods of Soils for Highway Engineering. 1st ed. China Communications Press: Beijing, China, 2020; 122–127, 213–217.

30. *NEN 7375-2004*; Leaching Characteristics—Determination of the Leaching of Inorganic Components from Moulded or Monolitic Materials with a Diffusion Test—Solid Earthy and Stony Materials. Milieukwaliteit: Amsterdam, The Netherlands, 2004.

31. Huang, Z.; Su, X.; Zhang, J.; Luo, D.; Chen, Y.; Li, H. Study on leaching of heavy metals from red mud-phosphogypsum composite materials. *Inorg. Chem. Ind.* **2022**, *54*, 133–140. [CrossRef]

32. Rong, S. Study on the Leaching Behavior of Rare Metals in Red Mud under pH-Influenced Conditions. Master's Thesis, Southwest Jiaotong University, Chengdu, China, 2020.

33. Sun, Z. Study on the Engineering Technology and Environmental Impacts of the Bayer Method of Filling Roadbeds with Red Mud. Master's Thesis, Shandong University, Jinan, China, 2017.

34. Li, Y. Research on Road Use Technology of Industrial Waste Red Mud. Master's Thesis, Chongqing Jiaotong University, Chongqing, China, 2021.

35. Zhang, X.; Fu, L. Application of cement stabilized aggregates in municipal projects. *Heilongjiang Sci. Technol. Inf.* **2008**, *10*, 190.

36. Zhao, Y. Experimental Study on Regeneration of Subgrade Phosphogypsum Lime Stabilized Soil. Master's Thesis, Jiangsu University, Zhenjiang, China, 2008.

37. Lu, H. Development of New Soft Soil Curing Agent and Research on Its Reaction Mechanism. Master's Thesis, Jinan University, Guangzhou, China, 2006.

38. Zhang, J.; Huang, Z.; Su, X.; Chen, Y.; Li, H.; Li, W. Effect of phosphogypsum addition on properties of red mud-phosphogypsum composites. *China Nonferrous Metall.* **2023**, *52*, 121–130. [CrossRef]

39. Cho, J.H.; Eom, Y.K.; Lee, T.G. Stabilization/solidification of mercury-contaminated waste ash using calcium sodium phosphate (CNP) and magnesium potassium phosphate (MKP) processes. *J. Hazard. Mater.* **2014**, *278*, 474–482. [CrossRef]